New measurement and reevaluation of the nuclear magnetic and quadrupole moments of ^{8}Li and ^{9}Li

D. Borremans,[1] D. L. Balabanski,[1,*] K. Blaum,[2,3] W. Geithner,[3] S. Gheysen,[1] P. Himpe,[1] M. Kowalska,[3] J. Lassen,[3,†] P. Lievens,[4] S. Mallion,[1] R. Neugart,[3] G. Neyens,[1] N. Vermeulen,[1] and D. Yordanov[1]

[1]*Instituut voor Kern- en Stralingsfysica, K.U.Leuven, B-3001 Leuven, Belgium*

[2]*PH Department, CERN, CH-1211 Geneva 23, Switzerland*

[3]*Institut für Physik, Universität Mainz, D-55099 Mainz, Germany*

[4]*Laboratorium voor Vaste-Stoffysica en Magnetisme, K.U.Leuven, B-3001 Leuven, Belgium*

(Received 30 June 2005; published 25 October 2005; publisher error corrected 3 November 2005)

The nuclear magnetic moment of ^{9}Li and the quadrupole moments of ^{8}Li and ^{9}Li have been measured by use of the β-asymmetry detection of nuclear magnetic resonance on optically polarized beams at ISOLDE/CERN. The radioactive beams were implanted in Si for g-factor measurements and in Zn, $LiNbO_3$, and $LiTaO_3$ crystals for quadrupole moment measurements. The electric-field gradient $V_{zz} = 4.26(4) \times 10^{15}$ V/cm^2 is deduced for Li in Zn. Using a recently adopted reference value, $Q(^{7}\mathrm{Li}) = -40.0(3)$ mb, we reevaluated all earlier reported nuclear quadrupole moments of ^{8}Li and ^{9}Li. Based on all available previous and present data, the adopted quadrupole moments for these isotopes are $Q(^{8}\mathrm{Li}) = +31.4(2)$ mb and $Q(^{9}\mathrm{Li}) = -30.6(2)$ mb. The magnetic moment of ^{9}Li is deduced as $\mu(^{9}\mathrm{Li}) = 3.43678(6)\mu_N$. The values are compared with predictions from shell-model and cluster-model calculations.

DOI: 10.1103/PhysRevC.72.044309 PACS number(s): 21.10.Ky, 27.20.+n

I. INTRODUCTION

The Li isotopes, among them the two-neutron halo nucleus ^{11}Li, belong to the most investigated nuclei of the past two decades. Because of their small nucleon number, the calculation of their properties can now be done by use of *ab initio* no-core shell-model approaches with realistic nucleon-nucleon interactions [1,2]. Cluster models, considering, e.g., the halo nucleus ^{11}Li as consisting of a ^{9}Li core and two neutrons [3] or an $\alpha+t+4n$ configuration [4], as well as models based on antisymmetric molecular dynamics (AMD) wave functions [5], are also used to describe these light nuclei. Accurate values of the nuclear ground-state properties of the Li isotopes, such as the magnetic dipole and electric quadrupole moments, are ideal tools for testing the validity of these nuclear models. Our final goal is to study these properties for the ^{11}Li halo nucleus, the most challenging case for both theory and experiment. As an intermediate result, we report here on the experimental procedures used to obtain improved values of the ^{8}Li and ^{9}Li dipole and quadrupole moments. Results for ^{11}Li, which were obtained recently, will be reported and discussed in a forthcoming paper.

Spin-polarized beams of Li isotopes are implanted into suitable crystals, where they decay with an asymmetric angular distribution of the emitted β particles. To allow for accurate nuclear-magnetic-resonance (NMR) measurements, several host crystals were investigated to find the best conditions for preserving the polarization, for achieving narrow resonance signals, and for finding suitable electric-field gradients (EFGs) for the determination of quadrupole moments. This is described in Sec. III A.

In Sec. III B, we describe the precise measurement of the magnetic moment of ^{9}Li relative to that of ^{8}Li. The ratio of their Larmor frequencies is measured by the β-asymmetry detection of NMR (hereafter β-NMR) with an accuracy reaching the 10^{-5} level, similar to that of the adopted magnetic moment of ^{8}Li [6,7].

For the determination of quadrupole moments, as described in Secs. III C and III D, we aim at measuring very precisely $Q(^{8}\mathrm{Li})$ and $Q(^{9}\mathrm{Li})$ relative to the quadrupole moment of ^{7}Li. Quadrupole moments reported in literature are given with respect to different reference values for ^{7}Li, for which more precise values have become available over time. Recently, the quadrupole moment of ^{7}Li was reevaluated based on refined calculations of EFGs [8]. The deduced value is in excellent agreement with a reevaluation of former nuclear scattering data [9] and the recommended value is $Q(^{7}\mathrm{Li}) = -40.0(3)$ mb [10]. In this paper, we reevaluate all earlier reported values for the ^{8}Li quadrupole moment, which were deduced from quadrupole frequencies measured in crystals of $LiNbO_3$ [11–13], $LiIO_3$ [11], and $LiTaO_3$ [14], relative to those measured for ^{7}Li [11,15–17]. We compare these results with our own values, which we obtained in two independent experimental runs and measured in two crystals: $LiNbO_3$ and $LiTaO_3$. A new adopted value for $Q(^{8}\mathrm{Li})$ is deduced, which is then used to determine the EFG of Li in Zn to the 1% level.

For ^{9}Li, earlier measurements were performed only in $LiNbO_3$ crystals [13,18], and the data do not agree very well with each other. In the present work, the quadrupole moment of ^{9}Li is measured relative to that of ^{8}Li in crystals of Zn and $LiTaO_3$. These results are compared with the earlier work, and a recommended value is deduced.

*On leave from St. Kliment Ohridski University of Sofia, BG-1164 Sofia, Bulgaria; present address: Dipartimento di Fisica, Universitá degli Studi di Camerino, I-62032 Camerino, Italy.

†Present address: TRIUMF ISAC, 4004 Wesbrook Mall, Vancouver, British Columbia, V6T 2A3 Canada.

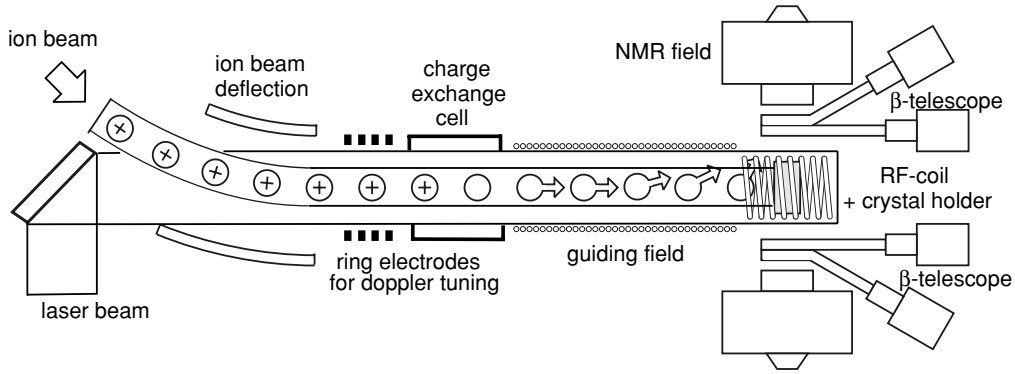

FIG. 1. Schematic view of the experimental setup. See text for details.

Finally, the revised quadrupole moments of the Li isotopes from $A = 6$ to $A = 11$ are compared with recent nuclear-model calculations.

II. EXPERIMENTAL SETUP AND MEASURING PROCEDURE

The experiment was performed at the on-line collinear laser spectroscopy beam line at the ISOLDE [19] facility at CERN. A 1.4-GeV pulsed proton beam (one pulse every 2.4 s with a maximum intensity of 3×10^{13} protons/pulse), provided by the PS Booster, is impinging on the ISOLDE production target. The target consists of a stack of rolled Ta foils. The Li isotopes, with half-lives $T_{1/2}(^8\mathrm{Li}) = 838(6)$ ms and $T_{1/2}(^9\mathrm{Li}) = 178.3(4)$ ms, are ionized on a hot tungsten surface and accelerated to an energy of 60 keV. Beams of 8×10^7 ^{8}Li and 4×10^6 ^{9}Li ions/pulse were selected by use of magnetic mass separation. Isobaric contamination was not an issue because isobars are either nonexistant (^{8}Be, ^{9}B), very exotic (^{8}B), or stable (^{9}Be). The Li beams were guided to the experimental setup, where they are overlapped collinearly with a continuous wave (cw) laser beam (Fig. 1) [20].

Polarization of the Li isotopes is achieved by optical pumping on a beam of neutral Li atoms. Therefore the Li^+ beam is neutralized by charge exchange with Na atoms in a vapor cell containing Na metal heated to about 250°C (leading to about 50% neutralization efficiency). The remaining ions are deflected out of the atom beam to prevent them from contributing as a nonoriented background to the subsequent β-asymmetry detection. A narrow-bandwidth cw dye laser (Coherent 699-21) with 4-dicyanomethylene-2-methyl-6-(*P*-dimethylaminostyryl)-4*H*-pyran laser dye provides circularly polarized light at a wavelength of 670 nm and a power of about 100 mW. This laser light induces resonant excitations between hyperfine-structure levels in the transition $2s\ ^2S_{1/2} - 2p\ ^2P_{1/2}$ of the Li atoms [D1 line, Fig. 2(a)]. With the neutralization cell at a tunable electrical potential of maximum ±10 kV, the velocity of the Li ion beam can be adjusted, which allows the Doppler tuning of the atomic excitation frequencies into resonance with the laser light. After several cycles of resonant excitation ($\Delta m = +1$) and subsequent decay ($\Delta m = 0, \pm1$), atomic and nuclear spin polarization is created. This process of "optical pumping" [21] needs an interaction time of typically 0.5 μs to reach maximum atomic polarization. The quantization axis is established by a small ($B_s \approx 1$ mT) guiding magnetic field $\vec{B}_s$ along the beam line. In a gradually increasing rotational field close to the NMR magnet, the coupled system of electronic and nuclear spins is rotated to the transverse direction, before both spins are adiabatically decoupled while entering the transversal static NMR field of $B_0 \approx 0.29$ T. Here the atoms are implanted into a suitable crystal, the nuclei thus forming a spin-polarized ensemble.

When the β-decay asymmetry is measured as a function of the Doppler-tuning voltage, the Li atoms are tuned into resonance with the laser light, so that the optical-pumping condition is established in the transitions between the hyperfine-structure components [see Fig. 2(b)]. The nuclear spin polarization is observed with two β-detection telescopes, each consisting of two plastic scintillators of 1-mm thickness,

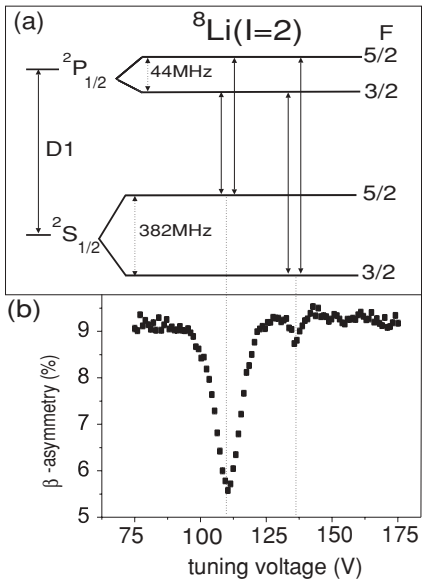

FIG. 2. (a) Atomic level scheme of ^{8}Li. (b) Example of a "hyperfine scan" in which the velocity of the Li atoms is Doppler tuned across the optical resonance by scanning the post-acceleration voltage of the ion beam. Only the ground-state hyperfine structure is clearly resolved.

placed at 0° and 180° with respect to $\vec{B}_0$. Comparison of the coincident count rates in the two telescopes allows one to deduce the asymmetry $a = (N_0 - N_{180})/(N_0 + N_{180})$, which is proportional to the nuclear spin polarization. Note that the observed asymmetries, as shown on the measured spectra, include an offset from instrumental asymmetries. The implantation depth of the 60-keV atom beam varies between 0.2 and 0.5 μm for the different crystals. Thus the surfaces of the crystals need to be carefully polished and treated to preserve the spin polarization and to ensure a well-defined EFG at the implantation site. All experiments are performed at room temperature.

Once the polarization condition is established, the voltage is set to the value yielding maximum β asymmetry. Now the nuclear moments can be measured with high precision by use of the β-NMR. For this purpose, a magnetic rf field with variable frequency $\nu_{\rm rf}$ perpendicular to the static magnetic field $\vec{B}_0$ is applied to the implanted ensemble.

For nuclei implanted into a crystal with cubic lattice symmetry, the nuclear Zeeman interaction with the static magnetic field causes an equidistant splitting of the magnetic substates m. If the applied frequency $\nu_{\rm rf}$ matches the Larmor precession frequency $\nu_L = g\mu_N B_0/h$, transitions are induced among all these states, resulting in a resonant destruction of the initial polarization [22].

If the crystal has a noncubic lattice symmetry, the electric quadrupole interaction causes an additional shift of the m levels [see Fig. 3(a)]. For a small angle γ between the static-field axis and the symmetry axis of the EFG, and $\nu_L \gg \nu_Q$ with $\nu_Q = eQV_{zz}/h$ being the quadrupole frequency, the energy levels are given by [22]

$$E_m = -mh\nu_L + \frac{h\nu_Q}{4I(2I-1)}[3m^2 - I(I+1)]\frac{3\cos^2\gamma - 1}{2}. \quad (1)$$

Resonant destruction of part of the initial polarization is induced by every frequency that fulfills the condition $h\nu_{\rm rf} = \Delta E = |E_m - E_{m-1}|$ [22,23]. The quadrupole frequency is deduced from the distance Δ between the $2I$ equidistant resonance frequencies [Figs. 3(a) and 3(b)]. The angle $\gamma \approx 0°$ is chosen in all our experiments. A deviation from perfectly collinear magnetic and electric interactions reduces the observed quadrupole frequency, e.g., by 1.1% for $\gamma = 5°$. Thus the possibility of misalignment may induce a systematic error on the deduced quadrupole moment. To control and minimize this error, all measurements were performed in two experimental runs, with the crystals mounted independently.

The destruction of polarization is in all cases measured by the recording of the β asymmetry as a function of the rf frequency, with the static-magnetic-field strength B_0 kept constant. In the case of a cubic crystal lattice, one resonance is observed for $\nu_{\rm rf} = \nu_L$, whereas in a crystal with an EFG the $2I$ equidistant resonances are symmetric with respect to the Larmor frequency and have a spacing of $\Delta = 6\nu_Q/[4I(2I-1)]$. The amplitudes of the resonances, being proportional to the destruction of polarization, are much smaller in the latter case, because only the population differences of

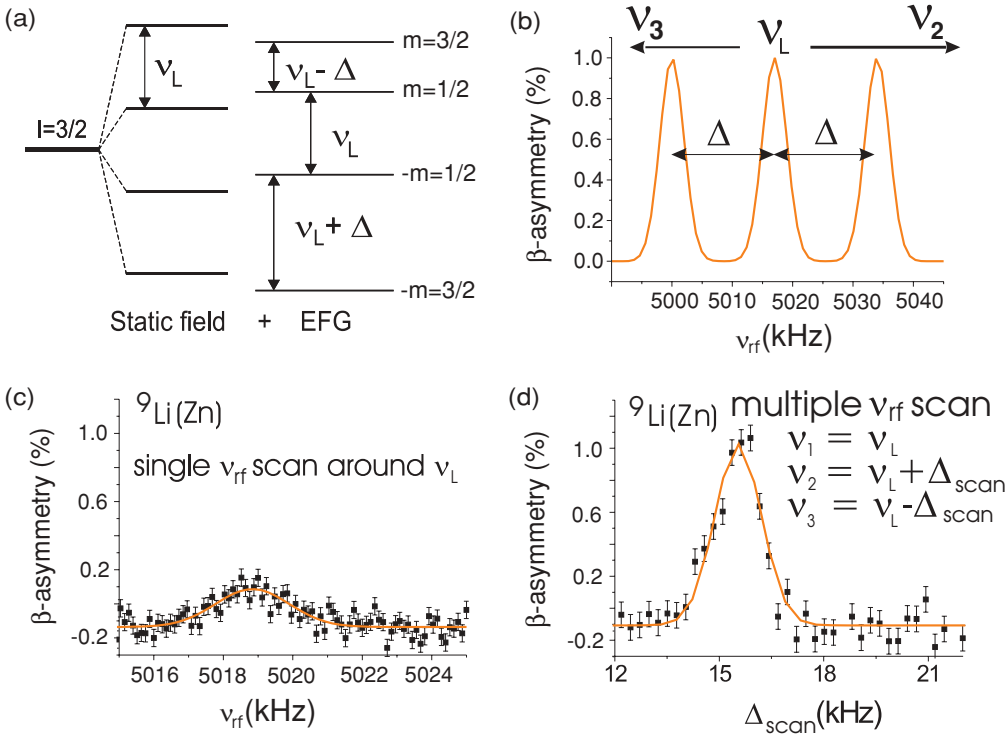

FIG. 3. (Color online) (a) Magnetic substates of a nucleus with spin $I = 3/2$ immersed into a static magnetic field and an EFG. (b) Simulation of the three resonances appearing in the β-decay asymmetry because of a resonant breakdown of the ensemble polarization. (c) Result of a single-frequency scan around the Larmor frequency for ^{9}Li implanted into a Zn crystal. (d) Multiple-rf scan for ^{9}Li in Zn.

two magnetic substates contribute to the signals. To overcome this problem, up to $2I$ rf fields with correlated frequencies can be applied simultaneously, as explained in [24] and in Figs. 3(a) and 3(b) for the case of ^{9}Li ($I = 3/2$). When three rf frequencies with values as defined in Fig. 3(d) are applied, all levels are coupled at once, resulting in one resonance with an amplitude that is more than five times larger than in the single-rf measurement shown in Fig. 3(c).

III. EXPERIMENTAL RESULTS

A. Choice of the implantation crystal

The implantation properties of the Li isotopes in a particular crystal lattice determine the linewidths and amplitudes of the observed β-NMR resonances. A long relaxation time, a homogeneous magnetic-field distribution over the crystal, and implantation of the isotope in a substitutional lattice site are prerequisites for a large β-NMR amplitude and narrow linewidth. To identify the optimal crystal for the implantation of Li isotopes, as well as to obtain a crystal-independent determination of the quadrupole moments, measurements were performed for ^{8}Li implanted into different single crystals: LiF, Si, Au with a cubic lattice structure, and Zn, $LiTaO_3$, and $LiNbO_3$ with an axially symmetric EFG.

In Fig. 4(a) the NMR amplitudes from measurements on ^{8}Li in Si, Au, and LiF are plotted as functions of the rf field strength. On the axis we put the field strength induced by the coil, not the one that is actually felt by the Li isotopes: Because of the skin effect this field strength is reduced in Si, Au, and Zn. The destroyed asymmetry (filled symbols) is compared with the laser-induced asymmetry as deduced from the hyperfine scan (open symbols). The asymmetry maintained after implantation (open symbols) is different in each crystal because of the different relaxation behavior. It is maintained best in LiF, which has a long relaxation time, $T_1 > 15$ s, at room temperature [25]. The asymmetry in the Au crystal is significantly reduced because of the fast Korringa relaxation in metals $\{T_1 = 0.6(3)$ s for Li in Au [26]$\}$. In addition, we see that in Au only about half of the initial polarization is destroyed at the Larmor frequency, whereas for the other crystals this ratio is about 80%. This means that in Au half the nuclei do not contribute to the NMR effect because they are implanted in defect-associated lattice sites with a noncubic environment.

In Fig. 4(b) the linewidths of the resonances are shown. In Si it is very small and dominated by homogeneous broadening that gives a purely Lorentzian line shape. An inhomogeneous broadening, induced, e.g., by a nonhomogeneous magnetic field or a small EFG, would lead to a more Gaussian shape, as observed in LiF. The fact that for low rf power the linewidth in Si is reduced to 0.5 kHz confirms that the applied static magnetic field is very homogenous over the beam spot, which is about 6 mm in diameter. Because of this small linewidth and large amplitude of the NMR signal in Si, this crystal was used for the measurement of the nuclear magnetic moment of ^{9}Li relative to that of ^{8}Li.

Figure 5 shows results of the same study for the crystals with a noncubic lattice symmetry: Zn, $LiTaO_3$, and $LiNbO_3$.

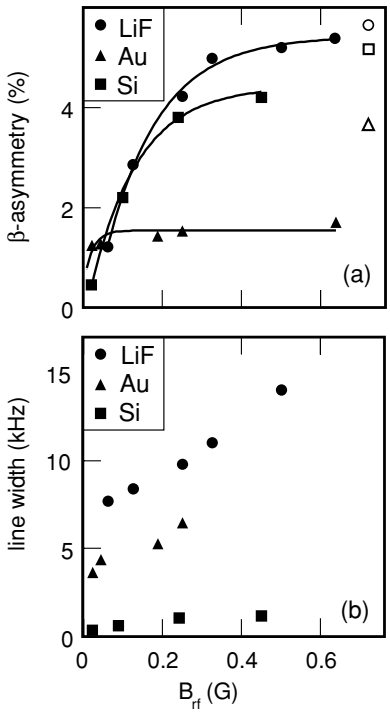

FIG. 4. (a) Amplitude and (b) linewidth of β-NMR resonances for ^{8}Li implanted in different crystals with cubic lattice symmetry as functions of the applied rf field strength. In (a) the laser-induced β-asymmetry after implantation (open symbols) is compared with the amplitudes of the NMR signals (filled symbols).

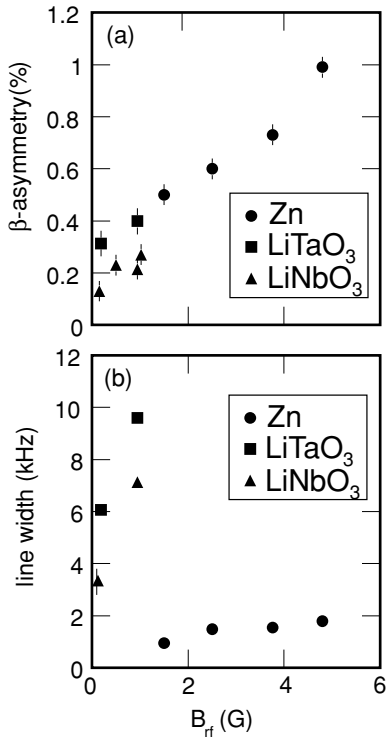

FIG. 5. (a) Amplitude and (b) linewidth of the ^{8}Li single-rf resonances as functions of the rf field strength in different implantation crystals with noncubic lattice symmetry.

As in Si, in Zn the linewidth of the resonance is mainly determined by homogeneous broadening, and at low power it is reduced to less than 1 kHz. In combination with the large-resonance amplitudes, this makes Zn a good crystal for accurate quadrupole frequency measurements on the Li isotopes. To deduce absolute values for the quadrupole moments, a reliable value for the EFG of Li in Zn is needed. As this EFG was determined to an accuracy of 6% only [27], we calibrate it for the determination of the quadrupole moment of ^{9}Li by measuring $\nu_Q(^8\text{Li in Zn})$ and $\nu_Q(^9\text{Li in Zn})$ and by using our newly adopted accurate value of the ^{8}Li quadrupole moment. A similar study is performed in the $LiTaO_3$ crystal. Although here the resonances are broader (≈6–10 kHz), the large EFG and large-resonance amplitudes still allow rather accurate measurements.

Measurements in two different $LiNbO_3$ crystals showed a significant difference in the observed resonance linewidths. The resonances were resolved for only one crystal, which illustrates that the crystal quality (as provided by the manufacturer) plays a crucial role. These resonances also suffered from small amplitudes, and therefore measurements were performed only for ^{8}Li in $LiNbO_3$, mainly for comparison with former such measurements.

To judge possible systematic effects, all the relevant measurements described in the following subsections were performed twice, in two beam time periods with independent magnetic-field calibrations and settings of the crystal orientation (referred to as run-1 and run-2).

B. Magnetic moment of ^{9}Li

The Larmor frequency of ^{9}Li ($I^\pi = 3/2^-$) was measured relative to that of ^{8}Li ($I^\pi = 2^+$), yielding the ratio of both g factors. Consistent values for the ^{8}Li magnetic moment have been reported [6,26,28], with the most precise numbers given by Winnacker *et al.* [6]. Here we use the value adopted in the compilation of Raghavan [7], $\mu = +1.653560(18)\,\mu_N$, corresponding to $g = 0.826780(9)$, for deducing the g factor of ^{9}Li.[1]

Both isotopes, ^{8}Li and ^{9}Li, were implanted alternately in the Si crystal, and for each of them more than 15 resonances were measured in each of the two runs. Typical resonances, obtained in a few minutes of beam time, are shown in Fig. 6.

The ratios of the Larmor frequencies, deduced as the weighted mean of the data in each run, are in very good agreement with each other, being 2.77124(6) and 2.77121(4), respectively. The weighted average of these gives a very precise value for the ratio of the g factors: $g(^9\text{Li})/g(^8\text{Li}) = 2.77122(3)$, from which we obtain $g(^9\text{Li}) = 2.29119(4)$. Thus

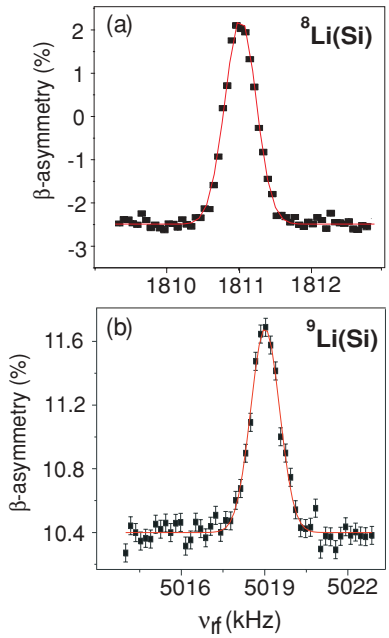

FIG. 6. (Color online) Examples of β-NMR spectra. The β asymmetry as a function of the rf is shown for ^{8}Li and ^{9}Li in Si. In (a) the error bars are too small to be visible.

the magnetic moment for ^{9}Li is $\mu(^9\text{Li}) = 3.43678(6)\,\mu_N$ in good agreement with the value $\mu = 3.4334(52)\,\mu_N$ reported by Arnold *et al.* [13]. An earlier value reported by Correll *et al.* [18], $\mu = 3.4391(6)\,\mu_N$, deviates by nearly 4σ from ours. However, our reevaluation of the results presented in that paper indicates that the errors quoted for these data may be underestimated.

C. Quadrupole moment of ^{8}Li; EFG of Li in Zn

In Table I, the earlier published values for the ^{8}Li quadrupole frequencies in single crystals of $LiNbO_3$, $LiTaO_3$, and $LiIO_3$ are summarized. The deduced quadrupole moments have been reevaluated, with common references used for the ^{7}Li quadrupole frequencies [11,15–17], and the new adopted ^{7}Li quadrupole moment [10]. All values agree with each other within their respective error bars.

We compare these previous results to the new values obtained in this work. A total of six quadrupole resonance spectra for ^{8}Li in $LiTaO_3$ were taken in the two experimental runs. A typical result is shown in Fig. 7(a). The data are fitted assuming that the resonances are equidistant, with the distance represented by the quadrupole splitting Δ as deduced from Eq. (1). Equal linewidths are assumed, and it has been verified that this does not influence the deduced splitting within the fit error. The resulting frequencies with their statistical fit errors are summarized in Fig. 8(a). The weighted mean values from the two runs are in excellent agreement with each other: $\nu_Q(1) = 59.44(36)$ kHz and $\nu_Q(2) = 59.60(24)$ kHz. We also remeasured the quadrupole frequency in a $LiNbO_3$ single crystal, resulting in an average value $\nu_Q(^8\text{Li in LiNbO}_3) = 43.4(8)$ kHz [Fig. 7(b)].

[1] We note that this number deviates from the weighted average of the g factors quoted in the original paper by Winnacker *et al.* [6], after correction for diamagnetism. However, further corrections to that value are necessary, accounting for chemical shifts in the crystalline samples and for a revised reference g factor for protons in water. Assuming this to be included in the tabulated value [7], we still believe there should be an additional systematic error (of the order of the experimental error) coming from these corrections.

TABLE I. Overview of the revised quadrupole moments of ^{8,9}Li relative to $|Q(^7\text{Li})| = 40.0(3)$ mb.

	Crystal	$\nu_Q(^7\text{Li})$ (kHz)	$\nu_Q(^A\text{Li})$ (kHz)	$\lvert Q(^A\text{Li})\rvert$ (mb)	Reference
^{8}Li	$LiNbO_3$	54.5(5) [15]	43(3)	31.6(22)	[12]
	$LiNbO_3$		42.5(6)	31.2(6)	[13]
	$LiNbO_3$		44.68(88)	32.8(8)	[11]
	$LiNbO_3$		43.4(8)	31.9(7)	This work-run 1
	$LiIO_3$	36.4(5) [11]	29.24(36)	32.1(6)	[11]
	$LiTaO_3$	76.7(6) [16,17]	60.2(3)	31.4(4)	[14]
	$LiTaO_3$		59.44(36)	31.0(4)	This work-run 1
	$LiTaO_3$		59.60(24)	31.2(4)	This work-run 2
				31.4(2)	**Adopted value**
	Zn		33.5(20)		[27]
	Zn		32.32(7)	Used to deduce EFG	This work-run 1
	Zn		31.84(12)		This work-run 2
^{9}Li	$LiNbO_3$	54.5(5)	48.4(24)	35.5(18)	[18]
	$LiNbO_3$		37.4(13)	27.4(9)	[13]
	$LiTaO_3$	Relative to ^{8}Li	58.2(11)	30.7(6)	This work-run 1
	$LiTaO_3$		57.9(7)	30.5(4)	This work-run 2
	Zn	Relative to ^{8}Li	31.4(2)	30.5(3)	This work-run 1
	Zn		31.1(1)	30.7(2)	This work-run 2
				30.6(2)[a]	**Adopted value**

[a]In the error calculation on the weighted mean, we did not include the standard deviation from the two earlier less precise measurements. The weighted mean value itself remains the same, whether or not the earlier values are included.

To deduce the ^{8}Li quadrupole moment relative to that of ^{7}Li, we take the ratio of the measured frequencies with respect to the ^{7}Li quadrupole frequency (column 2 of Table I). In $LiTaO_3$ this frequency has been measured twice to a precision of about 1% [16,17], and we take the weighted mean of both values, $\nu_Q = 76.7(6)$ kHz, as a reference. For the quadrupole frequencies of ^{7}Li in $LiIO_3$ and $LiNbO_3$ we use the values reported in [11] and [15], respectively. The deduced quadrupole moments from the present work are in very good agreement with all previous measurements (Table I). The weighted mean of all these data results in the adopted value $Q(^8\text{Li}) = +31.4(2)$ mb, with the sign as determined by Jänsch *et al*. [29].

Measurements of the quadrupole frequency of ^{8}Li in Zn were performed to determine precisely the EFG of Li in Zn. A typical spectrum is shown in Fig. 7(c). The fitted quadrupole splittings deduced from measurements in the two runs are summarized in Fig. 8(b). The weighted mean of the data from each run, with the errors determined by the respective standard deviations and statistical errors, are $\nu_Q(1) = 32.32(8)$ kHz and $\nu_Q(2) = 31.84(12)$ kHz. Given the small error bars, the two results differ from each other, which suggests that the crystal was aligned differently with respect to the magnetic field in both runs (a misalignment of $\gamma = 5^\circ$ can account for the observed deviation).

Using the larger value of these measured quadrupole frequencies and the newly adopted value for the ^{8}Li quadrupole moment, we can deduce the EFG of Li in Zn to the 1% accuracy level. To account for a possible 3° misalignment of the crystal c axis with respect to the applied magnetic field, we add 0.13 kHz to the error and obtain $|\nu_Q(^8\text{Li in Zn})| = 32.3(2)$ kHz. This results in an EFG for Li in Zn, $V_{zz}(\text{Li in Zn})(1 - \gamma_\infty) = 4.25(4) \times 10^{15}$ V/cm^2, in good agreement with the value reported by Ohtsubo *et al*., $4.24(27) \times 10^{15}$ V/cm^2 [27].

D. Quadrupole moment of ^{9}Li

To determine the quadrupole moment of ^{9}Li as precisely as we did that of ^{8}Li, we determined the ratio of both quadrupole frequencies in two different crystals, $LiTaO_3$ and Zn. Because of the very small β-asymmetry parameter of ^{9}Li (less than 0.1), we used the multiple-rf method to improve the experimental sensitivity by almost an order of magnitude (as demonstrated in Fig. 3). A comparison of the quadrupole frequencies deduced from multiple-rf and single-rf measurements revealed no significant difference. Measurements were performed in both runs, and in the two crystals several scans were alternately made for ^{8}Li and for ^{9}Li. The fit results from each measurement are summarized in Fig. 8. The resulting quadrupole frequencies are given in Table I separately for the two runs and the two crystals. Typical multiple-rf resonance curves for ^{9}Li in Zn and in $LiTaO_3$ are shown in Fig. 9.

By use of our adopted value for $Q(^8\text{Li})$, these four independent measurements of the ratio $Q(^9\text{Li})/Q(^8\text{Li}) = \nu_Q(^9\text{Li})/\nu_Q(^8\text{Li})$ lead to the ^{9}Li quadrupole moments given in the last column of Table I. They are all consistent with each other and much more accurate than the earlier reported values deduced from measurements in a $LiNbO_3$ single crystal by Correll *et al*. [18] and by Arnold *et al*. [13].

As a recommended value we take the weighted mean of all independent measurements (Table I), leading to $Q(^9\text{Li}) = -30.6(2)$ mb, with the negative sign adopted from theory.

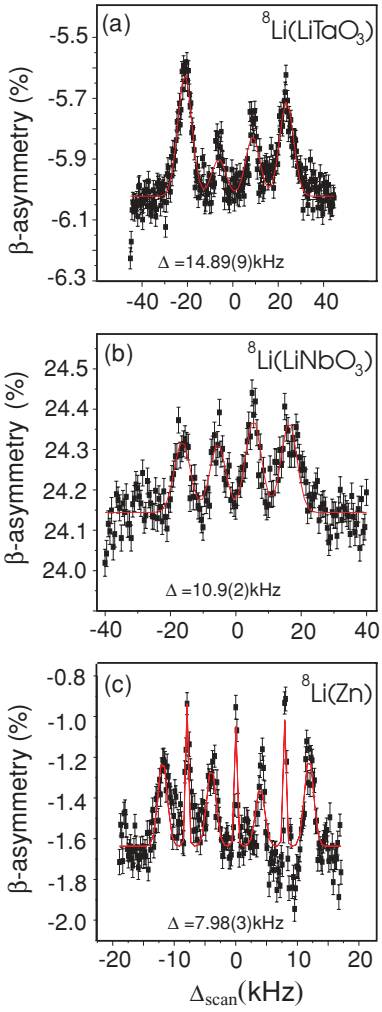

FIG. 7. (Color online) Examples of β-NMR spectra of ^{8}Li in different crystals with an EFG. The asymmetry is shown as a function of the frequency detuning, $\Delta_{scan} = \nu_{rf} - \nu_L$, with respect to the central Larmor frequency. Because of the narrow resonance linewidths in the Zn crystal, two-photon transitions are observed as well.

IV. DISCUSSION

In Table II we summarize the experimental results for the magnetic and quadrupole moments of all Li isotopes. The quadrupole moments are all directly or indirectly deduced relative to that of ^{7}Li, including that of ^{6}Li which was recently remeasured very precisely by Cederberg *et al.* [30]. The quadrupole moment of ^{11}Li was reported relative to that of ^{9}Li [24], and we reevaluate its absolute value based on the new accurate ^{9}Li quadrupole moment reported here.

In a shell-model picture, the properties of the odd-A Li isotopes with three protons are dominated by the unpaired proton in the $\pi p_{3/2}$ orbital. This is reflected in their g factors, which are all close to the Schmidt value $g_{sp}(\pi p_{3/2}) = 2.5293$, as shown in Fig. 10. For the odd-odd Li isotopes, ^{6}Li (I=1) and ^{8}Li (I=2), the neutron is expected to occupy preferentially the $\nu p_{3/2}$ orbit. Indeed, the free-nucleon g factor for a pure $\pi p_{3/2}\nu p_{3/2}$ configuration, coupled to spin $I = 1$

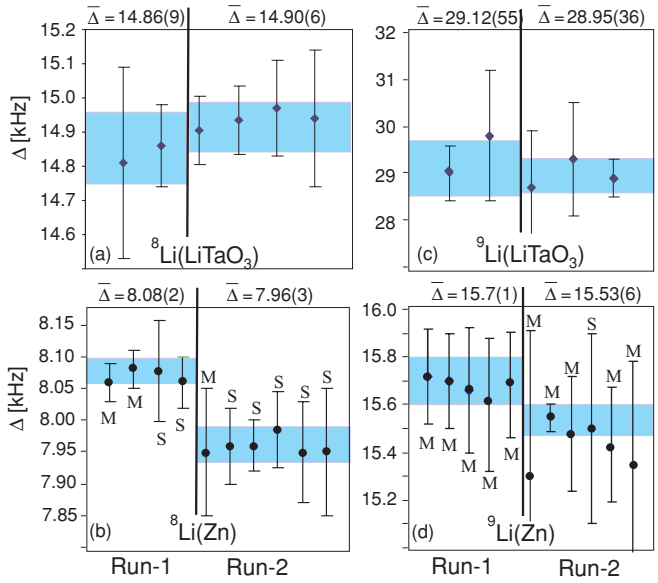

FIG. 8. (Color online) Overview of the deduced quadrupole splittings from fitting the individual NMR spectra. In the $LiTaO_3$ crystal we applied the single (S) NMR method for ^{8}Li and multiple (M) NMR for ^{9}Li. In the Zn crystal the two measuring techniques were applied for both isotopes, showing the independence of the results on the applied measuring procedure. The weighted mean of the data taken during each run is indicated by a gray bar (blue in the color version).

or $I = 2$, results in the value $g(\pi p_{3/2}\nu p_{3/2}) = 0.627$. The experimentally observed g factor for both isotopes is somewhat larger than this, around 0.823, which suggests that other configurations contribute to their wave function. For example, the g factor for a configuration with a neutron in the $\nu p_{1/2}$ orbital is $g(\pi p_{3/2}\nu p_{1/2}) = 2.84$, and a small admixture of

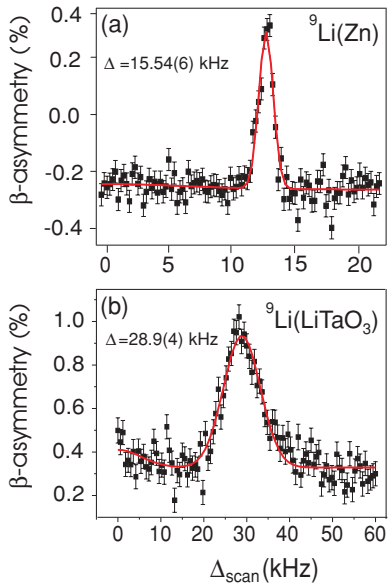

FIG. 9. (Color online) Examples of multiple-rf scans for ^{9}Li after implantation in (a) Zn and (b) $LiTaO_3$.

TABLE II. Experimental magnetic dipole and electric quadrupole moments of Li isotopes. The magnetic moments have been corrected for diamagnetic shielding. The quadrupole moments are all deduced relative to that of ^{7}Li.

Isotope	I^π	$\mu(\mu_N)$	Ref.	Q(mb)	Ref.
^{6}Li	1^+	0.8220473(6)	[7]	−0.806(6)	[30]
^{7}Li	$3/2^-$	3.256427(2)	[7]	−40.0(3)	[9]
^{8}Li	2^+	1.653560(18)	[7]	+31.4(2)	This work
^{9}Li	$3/2^-$	3.43678(6)	This work	−30.6(2)	This work
^{11}Li	$3/2^-$	3.668(3)	[20]	−35.0(49)	[24]

this component in the wave function can easily explain the observed differences. This is confirmed from shell-model calculations, which predict indeed some occupation of the $\nu p_{1/2}$ and also of the $\pi p_{1/2}$ orbits and do reproduce the observed g factor within a few percent (open circles in Fig. 10).

We performed the shell-model calculation with the CKI (Cohen-Kurath) interaction [31], in which protons and neutrons are restricted to the p shell. Free-nucleon g factors were used to calculate magnetic moments and effective charges $e_\pi = 1.35e$ and $e_\nu = 0.5e$ to calculate the quadrupole moments. Although this model space and interaction seem to account rather well for the g factors, they do not reproduce the observed trend in the quadrupole moments (see open circles in Fig. 11). The strong increase of the absolute value of the ^{7}Li quadrupole moment compared with that of ^{9}Li is not at all reproduced in this model space. If ^{7}Li is considered as a two-cluster structure of ^{4}He and ^{3}H, then the enhanced quadrupole moment is reproduced well, $Q_{\rm clu} = -38.5$ mb [32]. Recently, a microscopic cluster-model calculation was performed for all Li isotopes up to $A = 11$ by use of the stochastic variational method [4,33]. In this model, ^{7,8,9,11}Li are considered to consist of ^{4}He, ^{3}H, and single-neutron clusters. The calculated quadrupole moments for the odd isotopes are represented in Fig. 11 by filled squares. They reproduce very well the trend line of the experimental values, in particular between ^{7}Li and ^{9}Li. For ^{11}Li, an increase in the quadrupole moment is predicted, but a more accurate experimental value is needed to prove this to be correct. By performing such an experiment in a Zn crystal, one can improve the error on the ^{11}Li quadrupole moment by an order of magnitude as compared with the earlier value that was obtained by use of a $LiNbO_3$ host.

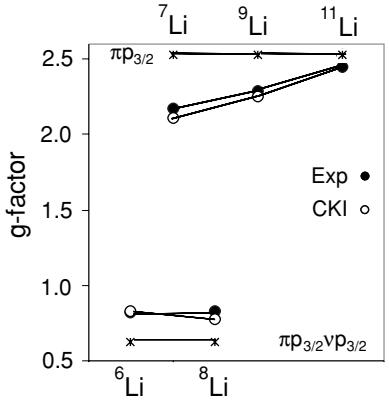

FIG. 10. g factors of Li isotopes, compared with Schmidt values and to a shell-model calculation developed by Cohen and Kurath [31] interaction in the p shell with free-nucleon g factors.

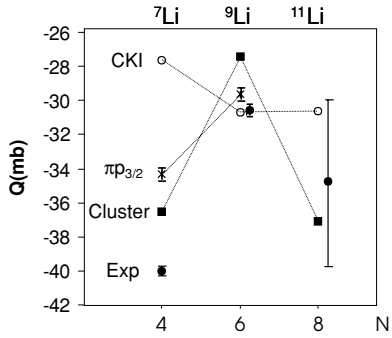

FIG. 11. Experimental quadrupole moments of odd-A Li isotopes, compared with a shell-model calculation (with CKI interaction in the p shell), with multicluster-model calculations, and with the value for a pure $\pi p_{3/2}$ configuration ($e_\pi = 1.35e$ and $e_\nu = 0.5e$.), assuming that the Li quadrupole moments are determined by the unpaired proton only.

This cluster model also predicts very well the recently observed decrease of the charge radii from $A = 6$ to $A = 9$ [34]. Using the experimental charge radii and assuming that the quadrupole moment of the odd-A isotopes is determined only by the $p_{3/2}$ proton, we can calculate their single-particle quadrupole moment as $Q_{\rm sp} = -e_{\rm eff}[(2j-1)/(2j+2)]\langle r^2(N)\rangle$. With an effective charge $e_\pi = 1.5e$, these single-particle values (stars in Fig. 11) reproduce the experimental values rather well. This confirms that indeed the unpaired proton gives the major contribution to the odd-A Li quadrupole moments. The agreement is not as good for ^{7}Li because of the enhanced cluster effect in this nucleus, which needs to be considered explicitly to account for the quadrupole moment observed.

V. CONCLUSION

The implantation of ^{8}Li and ^{9}Li into Si allowed the determination of the magnetic moment of ^{9}Li with a similar accuracy as for ^{8}Li: $\mu(^9\text{Li}) = 3.43678(6)\,\mu_N$. By implantation of these isotopes into $LiTaO_3$ and Zn single crystals, we could determine their quadrupole moments to a relative accuracy of 1%, which is an improvement of nearly an order of magnitude for $Q(^9\text{Li})$. Our experimental values are compared with earlier measured quadrupole moments after they were all renormalized to the same reference value $Q(^7\text{Li}) = -40.0(3)$ mb. This yields new adopted values $Q(^8\text{Li}) = +31.4(2)$ mb and $Q(^9\text{Li}) = -30.6(2)$ mb. These accurate nuclear moments are compared with results of shell-model and cluster-model calculations. Good agreement is found with the predictions of the cluster model, in particular in explaining the large enhancement of the magnitude of the ^{7}Li quadrupole moment. A more accurate value for the EFG of Li implanted in Zn, $V_{zz}(1-\gamma_\infty) = 4.25(4) \times 10^{15}$ V/cm^2, was obtained.

ACKNOWLEDGMENTS

The authors thank the ISOLDE technical group for their assistance during the experiment. This work was supported by the German Ministry for Education and Research (BMBF) under contracts 06 MZ 175 and 06 MZ 962 I, by the Interuniversity Attraction Pole (IAP) project p5–07 of the Belgian Science Policy Office. P.H. acknowledges support from the Institute for the Promotion of Innovation through Science and Technology in Flanders (IWT-Vlaanderen).

[1] P. Navratil and B. R. Barrett, Phys. Rev. C **57**, 3119 (1998).
[2] P. Navratil and E. W. Ormand, Phys. Rev. C **68**, 034305 (2003).
[3] P. Descouvement, Nucl. Phys. **A626**, 647 (1997).
[4] K. Varga, Y. Suzuki, and R. G. Lovas, Phys. Rev. C **66**, 041302(R) (2002).
[5] Y. Kanada-En'yo and H. Horiuchi, Prog. Theor. Phys. Suppl. **142**, 205 (2001).
[6] A. Winnacker, D. Dubbers, F. Fujara, K. Dörr, H. Ackermann, H. Grupp, P. Heitjans, A. Körblein, and H.-J. Stöckmann, Phys. Lett. **A67**, 423 (1978).
[7] P. Raghavan, At. Data Nucl. Data Tables **42**, 189 (1989).
[8] M. Urban and A. J. Sadlej, Chem. Phys. Lett. **173**, 157 (1990).
[9] H. G. Voelk and D. Fick, Nucl. Phys. **A530**, 475 (1991).
[10] P. Pyykkö, Mol. Phys. **99**, 1617 (2001).
[11] T. Minamisono, T. Ohtsubo, I. Minami, S. Fukuda, A. Kitagawa, M. Fukuda, K. Matsuta, Y. Nojiri, S. Takeda, H. Sagawa, and H. Kitagawa, Phys. Rev. Lett. **69**, 2058 (1992).
[12] H. Ackermann, D. Dubbers, M. Grupp, P. Heitjans, and H.-J. Stöckmann, Phys. Lett. **B52**, 54 (1974).
[13] E. Arnold, J. Bonn, W. Neu, R. Neugart, and E. W. Otten (ISOLDE Collaboration), Z. Phys. A **331**, 295 (1988).
[14] D. Dubbers, K. Dörr, H. Ackermann, F. Fujara, H. Grupp, M. Grupp, P. Heitjans, A. Körblein, and H.-J. Stöckmann, Z. Phys. A **282**, 243 (1977).
[15] T. K. Halstead, J. Chem. Phys. **53**, 3427 (1970).
[16] G. E. Peterson, P. M. Bridenbaugh, J. Chem. Phys. **48**, 3402 (1968).
[17] E. V. Charnaya, V. S. Kasperovich, M. N. Palatnikov, M. G. Shelyapina, C. Tien, and C. S. Wur, Ferroelectrics **234**, 223 (1999).
[18] F. D. Correll, L. Madansky, R. A. Hardekopf, and J. W. Sunier, Phys. Rev. C **28**, 862 (1983).
[19] E. Kugler, Hyperfine Interact. **129**, 23 (2000).
[20] E. Arnold, J. Bonn, R. Gegenwart, W. Neu, R. Neugart, E. W. Otten, G. Ulm, and K. Wendt, Phys. Lett. **B197**, 311 (1987).
[21] A. Kastler, J. Phys. (paris) **11**, 255 (1950).
[22] C. P. Slichter, in *Principles of Magnetic Resonance*, edited by M. Cardona, P. Fulde, and H.-J. Queisser (Springer-Verlag, Berlin, Heidelberg, New York, 1980).
[23] E. Matthias, B. Olson, D. A. Shirley, and J. E. Templeton, Phys. Rev. A **4**, 1626 (1971).
[24] E. Arnold, J. Bonn, A. Klein, R. Neugart, M. Neuroth, E. W. Otten, P. Lievens, H. Reich, and W. Widdra, Phys. Lett. **B281**, 16 (1992).
[25] M. I. Bulgakov, A. D. Gul'ko, Yu. A. Oratovskii, and B. B. Trostin, Sov. Phys. JETP **34**, 356 (1972).
[26] R. C. Haskell and L. Madansky, Phys. Rev. C **7**, 1277 (1973).
[27] T. Ohtsubo, Y. Nakayama, I. Minami, M. Tanigaki, S. Fukuda, A. Kitagawa, M. Fukuda, K. Matsuta, Y. Nojiri, H. Akai, and T. Minamisono, Hyperfine Interact. **80**, 1051 (1993).
[28] D. Connor and T. Tsang, Phys. Rev. **126**, 1506 (1962).
[29] H. J. Jänsch, M. Detje, H. D. Ebinger, W. Preyss, H. Reich, R. Veith, W. Widdra, D. Fick, M. Röckelein, and H.-G. Völk, Nucl. Phys. **A568**, 544 (1994).
[30] J. Cederberg, D. Olson, J. Larson , G. Rakness, K. Jarausch, J. Schmidt, B. Borovsky, P. Larson, and B. Nelson, Phys. Rev. A **57**, 2539 (1998).
[31] S. Cohen and D. Kurath, Nucl. Phys. **73**, 1 (1965); **A101**, 1 (1967) .
[32] H. Walliser and T. Fliessbach, Phys. Rev. C **31**, 2242 (1985).
[33] K. Varga, Y. Suzuki, and I. Tanihata, Phys. Rev. C **52**, 3013 (1995).
[34] G. Ewald, W. Nörtershäuser, A. Dax, S. Götte, R. Kirchner, H.-J. Kluge, Th. Kühl, R. Sanchez, A. Wojtaszek, B. A. Bushaw, G. W. F. Drake, Z.-C. Yan, and C. Zimmermann, Phys. Rev. Lett. **93**, 113002 (2004).